Mechanical Properties of Murine Leukemia Virus Particles: Effect of Maturation

Nitzan Kol,* Micha Gladnikoff,* David Barlam,† Roni Z. Shneck,‡ Alan Rein,§ and Itay Rousso*
*Department of Structural Biology, Weizmann Institute of Science, Rehovot, Israel; †Department of Mechanical Engineering and ‡Department of Materials Engineering, Ben-Gurion University of the Negev, Beer-Sheva, Israel; and §HIV Drug Resistance Program, National Cancer Institute–Frederick, Frederick, Maryland

ABSTRACT After budding from the host cell, retroviruses undergo a process of internal reorganization called maturation, which is prerequisite to infectivity. Viral maturation is accompanied by dramatic morphological changes, which are poorly understood in physical/mechanistic terms. Here, we study the mechanical properties of live mature and immature murine leukemia virus particles by indentation-type experiments conducted with an atomic force microscope tip. We find that both mature and immature particles have an elastic shell. Strikingly, the virus shell is twofold stiffer in the immature (0.68 N/m) than the mature (0.31 N/m) form. However, finite-element simulation shows that the average Young's modulus of the immature form is more than fourfold lower than that of the mature form. This finding suggests that per length unit, the protein-protein interactions in the mature shell are stronger than those in the immature shell. We also show that the mature virus shell is brittle, since it can be broken by application of large loading forces, by firm attachment to a substrate, or by repeated application of force. Our results are the first analysis of the mechanical properties of an animal virus, and demonstrate a linkage between virus morphology and mechanical properties.

INTRODUCTION

Enveloped retroviruses are complex and efficient ensembles that are highly evolved to spread infection. Importantly, a virion must satisfy several potentially conflicting demands during its lifetime—spontaneous assembly during budding, durability in the outside environment, and then efficient membrane fusion during entry into a target cell. As a result, the virus is likely to adopt a different set of physical properties at different stages of its lifecycle.

Expression of a single protein, termed Gag, is sufficient for formation of virus-like particles (1,2). After budding from the cell, virus particles undergo a maturation step essential for infectivity. Maturation is induced by the cleavage of the Gag protein by virus-encoded protease (PR) into at least three products: matrix (MA), capsid (CA), and nucleocapsid (NC) (3) (Fig. 1 *A*). The significance of maturation is indicated by the fact that current protocols for highly active antiretroviral therapy, used in treatment of HIV-1-infected individuals, generally include inhibitors of PR. Maturation has been extensively studied using biochemical methods and various electron microscopy (EM) imaging techniques (4). As observed by EM, maturation has no effect on the virus dimensions but has a striking visual effect on the internal virus structure (schematically shown in Fig. 1 *B*). Immature particles are characterized by a darkly stained ring under the virus envelope, whereas mature virus particles, after processing of Gag, exhibit an electron-dense core that is largely detached from the membrane (5–9). In addition, immature particles are far more stable under mild detergent treatment than are mature particles (7,10,11). However, nothing is known of the impact that maturation has on the structural and mechanical properties of live viruses. In parallel, characterization of the mechanical properties of virus particles may offer insight into their structure.

It is widely accepted that in mature particles, MA molecules are localized below the virus membrane, possibly in some sort of a lattice arrangement. Yet, there are many open questions associated with the structure and mechanical properties of this MA layer. In particular, is it a continuous lattice, or does it consist of disconnected patches? If the layer is continuous, is it rigid or soft and flexible? The existence of a rigid MA shell in mature particles would affect the energetic barriers associated with viral entry. According to current models, the energy required for pore formation between the virus and cell membranes is considered to be the main barrier for entry. Breakage of a rigid MA shell, if one exists, introduces an additional barrier for this process. Therefore, the study of the mechanical properties of virus particles is essential for understanding molecular mechanisms in virus replication.

An important model system for the study of retrovirus biology is the Moloney Murine Leukemia Virus (MLV), which is a member of the γ-retrovirus genus. Like other γ-retroviruses, MLV assembles at the plasma membrane. Here, we analyze the mechanical properties of mature and completely immature live MLV particles through indentation-type experiments conducted with an atomic force microscope (AFM) tip. AFM is uniquely suited to studying virus mechanical properties, since it combines high sensitivity in applying and measuring forces and high precision in positioning a tip relative to the sample with the ability to operate in physiological environments. Indeed, AFM has

Submitted December 19, 2005, and accepted for publication April 20, 2006.

Address reprint requests to Itay Rousso, Dept. of Structural Biology, Weizmann Institute of Science, Rehovot 76100, Israel. Tel.: 972-8-934-3479; Fax: 972-8-934-4136; E-mail: itay.rousso@weizmann.ac.il.

0006-3495/06/07/767/08 $2.00
doi: 10.1529/biophysj.105.079657

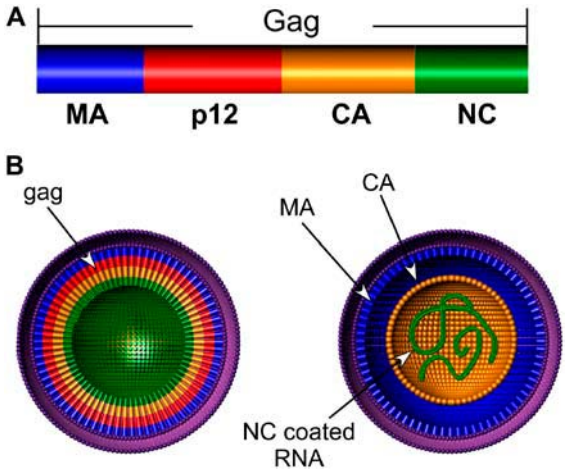

FIGURE 1 (*A*) Schematic representation of the MLV Gag protein. Blue, matrix domain (MA) of Gag; red, p12 domain of Gag protein; yellow, capsid domain (CA) of Gag; green, nucleocapsid domain (NC) of Gag protein. In the precleaved state these main domains are linked in a long polymer. (*B*) Schematic models for MLV mature and immature states. In the immature form, a thick layer, composed of Gag proteins, is observed beneath the membrane. Viral maturation is induced by the proteolytic processing of Gag into four domains: MA, p12 (not visible in mature particles), CA and NC, and their reassembly.

been successfully used to measure the mechanical properties of other biological samples (12–14), some as small as viruses, including bacteriophage capsid proheads (15), microtubules (16), and peptide nanotubes (17). The results reported here provide new insight into the structure of retrovirus particles. We also observed a clear difference in mechanical properties between the mature and immature particles. Moreover, this work establishes the groundwork for further investigation of a possible link between mechanical properties of a virus and biological function.

MATERIALS AND METHODS

Virus production and purification

Wild-type virus particles used in this study were of the infectious molecular clone of MLV termed pRR88 (18). Completely immature particles were produced by the D32L mutant in the active site of the PR coding region of pRR88 (18). Virus particles were produced by transfection of 293T cells with either the WT pRR88 or the D32L genome using standard calcium phosphate methods (19). The medium was replaced 18–24 h post-transfection and supernatants were harvested after two days. Virus-containing supernatants were cleared from cellular debris by centrifugation at 500 *g* for 5 min. Supernatants were purified by centrifugation through a sucrose cushion (20% sucrose in TNE buffer: 0.1 M NaCl, and 1 mM EDTA in 10 mM Tris buffered to pH 7.6) at 20,000 *g* for 90 min at 4°C. Virus pellets were then resuspended in TNE buffer.

Sample preparation for AFM imaging and force measurements

Microscope glass slides were cleaned by boiling in HCl solution, dried, and rendered hydrophobic in hexamethyldisilazane (HMDS) vapors to enable attachment of the virus particles (15). Virus particles were also attached, by electrostatic interactions, onto freshly cleaved mica pretreated with 20 mM $MnCl_2$. Before deposition, purified virus solutions were filtered through a 0.45 μm filter. A 10 μl droplet of virus supernatant was then deposited onto a glass slide or mica surface and left to absorb onto the substrate for 15 min. The glass or mica surface was then gently rinsed with TNE buffer to remove unbound material. All measurements were carried out under TNE buffer. Replacing TNE buffer with cell culture media (DMEM, 10% FCS, 25 mM Glucose, and 10 mM HEPES pH 7.4) had no effect on the results (data not shown).

AFM imaging and indentation experiments

All AFM experiments were carried out using a Bioscope with a Nanoscope IV controller (Veeco, Santa Barbara, CA) equipped with a dimension XY closed loop scanner mounted on an inverted optical microscope (Axiovert 200M, Carl Zeiss, Germany). Images of virus particles were acquired in AFM tapping mode in a fluid environment and rendered using the WSxM software (Nanotec Electronica, http://www.nanotec.es/progcorn.htm). Pyramidal silicon nitride triangular cantilevers (with a measured averaged stiffness of 0.2 N/m (DNP) or 0.6 N/m (MLCT-AUHW) for mature or immature viruses, respectively) were used, their spring constants being determined experimentally by measuring the thermal fluctuations of the cantilevers (20). Both cantilever types have a nominal tip radius of 20 nm. To measure the mechanical properties of an individual virus, an indentation experiment was performed with the microscope operated in the force-distance mode. Before beginning an indentation experiment, the probe was positioned at the center of the virus surface, and the AFM operation was switched from tapping to contact mode by reducing the driving amplitude to practically 0 mV. Thus, force-distance curves were carried out under contact mode operation. For each virus measurement, ~100 force-distance curves were performed at a scan rate of 0.5 Hz (corresponds to a loading rate of 95 nm/s). To avoid viral damage during an experiment, the deflection of the cantilever was maintained within the range of 150–200 mV, which corresponds to a maximal loading force of ~2 nN.

Data analysis for calculating the virus point stiffness

To obtain the point stiffness of a virus particle from a set of roughly 100 successive force-distance curves, each curve was shifted, first along the *z* axis to set the tip-sample contact point to a distance of zero, and then along the *y* axis to set deflection in the noncontact mode to zero. We further analyzed each experiment by plotting the individual measured point stiffness as a histogram (Fig. 3 *B*), and as a function of the measurement count (Fig. 3 *C*). Virus measured stiffness (k_{meas}) was derived mathematically from the slope of the force-distance curve. A linear function was fitted to the upper 75% of the force-distance curve (Fig. 3 *A*, *double-headed arrow*), except for virus particles having a height of 50 nm or less, in which case only the upper 25% was used. Virus particles whose point stiffness values decreased consistently during experimentation were discarded, since they underwent irreversible deformation, probably due to fatigue or even breakage. Next, a maximal deflection threshold value was set. Curves failing to reach this value were discarded, while the remaining aligned curves were averaged. The averaged force-distance curves were then converted from deflection units (V) to loading force (N) by multiplying by the deflection sensitivity (in nm/V, derived from a force-distance curve performed on mica) and the spring constant (N/m) of the cantilever. The virus's measured stiffness (k_{meas}, in N/m) was derived mathematically from the slope of the averaged force-distance curve, as described above. The measured stiffness comprises the stiffness constants of both the virus (k_{virus}) and the cantilever (k_{can}). Assuming that the system can be modeled as two springs arranged in a series, the point stiffness of the virus can be computed according to Hooke's law:

$$k_{virus} = \frac{k_{can} \times k_{meas}}{k_{can} - k_{meas}}.$$

All data analysis was carried out using MatLab software (The MathWorks, Natick, MA).

Finite element calculation

To calculate the Young's modulus from the measured virus stiffness we utilized the finite element method. The virus was modeled as a hollow sphere, made of a homogeneous material, resting on a flat rigid surface and loaded at a diametrically opposite point by an absolutely rigid spherical indenter with radius of 20 nm similar to the AFM tip used in the experiments. Sliding frictionless contact is assumed between the flat substrate and virus and between the indenter and the virus. This requires a solution of a nonlinear problem to find the distribution of forces in the contact area. The numerical model comprises a linear elastic material behavior and nonlinear geometric kinematics (allowing for large displacements). The resulting strains were found to be smaller than 1%, justifying the assumption of linear elastic behavior. This problem has been solved by the MSC.MARC software. Utilizing the axial symmetry of the problem, only a sector of 5° was modeled. The sectors are divided into 1600 and 7500 elements in the mature and immature models, respectively, and subjected to axisymmetrical boundary conditions. Loading was simulated by prescribing the downward movement of 2 nm of a rigid indenter, calculated in 20 concurrent increments. The stiffness of the model is calculated as the maximum force divided by the corresponding displacement. The Young's modulus of the model material was adjusted and the analysis repeated until the calculated rigidity fitted the measured one.

RESULTS AND DISCUSSION

Imaging virus particles

Virus particles were imaged in a TNE buffer environment with the AFM operated in tapping mode to minimize possible damage (Fig. 2 *A*). Particles were not treated in any way, and were kept as close as possible to their native state, except for their attachment onto a glass or mica substrate. In contrast to our experience using other methods, we found that precoating glass slides with HMDS vapors resulted in constructive virus attachment. Virus particles were attached strongly enough to the glass substrate to allow repetitive successful scans, while maintaining their native dimensions (80–150 nm) (9), as determined by their cross-sectional profiles (a cross section of a typical virus is shown in Fig. 2 *B*). Virus dimension was determined by their height rather than their width. The width of the virus is less accurate and appears to be larger than the height due to convolution between the AFM tip and the virus.

We also noted that when virus particles are deposited by electrostatic interactions onto positively charged mica, they are deformed. Analysis of their cross-sectional profiles shows that the height of these particles is 50 nm or less (data not shown), which is about half the diameter of the intact virus in solution. Excessive binding forces between the virus and the mica substrate are likely to cause the observed deformation. Finally, there were no visible differences between mature and immature particles, under all of the above imaging conditions (data not shown).

Indentation of virus particles

To measure the mechanical properties of virus particles, the AFM tip was positioned at the center of a single virus surface, and force-distance curves were acquired at the same position. To minimize drift of the AFM probe during experiments, an XY closed loop scanner was used. A typical force-distance curve for a mature virus particle is plotted in Fig. 3 *A*, together with the corresponding cantilever deflection curve. The cantilever deflection curve is obtained by measuring a force-distance curve for glass, which can be considered an infinitely stiff material compared to the cantilever, and one that the probe cannot deform in any way. The difference between the z displacement of the virus and the cantilever deflection for a given loading force corresponds to the indentation of the virus by the AFM probe. As seen in Fig. 3 *A*, even at the maximal applied loading force, the indentation depth was on the order of a few nanometers. Maintaining small indentation depths is essential for minimizing damage to the sample during the experiment. It also ensures that the rigid supporting substrate or the CA core (in mature virus particles) will not contribute significantly to the measured stiffness (21,22). Moreover, it is possible that

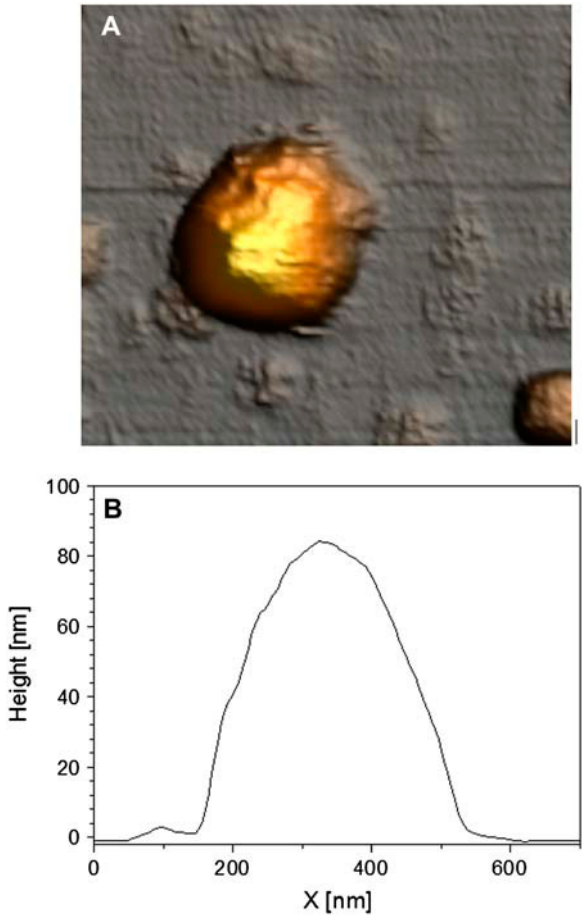

FIGURE 2 Moloney Murine Leukemia Virus particle shape and dimensions. (*A*) An AFM topographic image, acquired in tapping mode, of a mature MLV virus in TNE buffer (scan area 1 × 1 μm, 512 × 512 pixels). The virus particle is deposited on a microscope glass slide pretreated with HMDS vapors. (*B*) The cross-sectional profile of the virus particle revealing (from its height) its ~85 nm diameter.

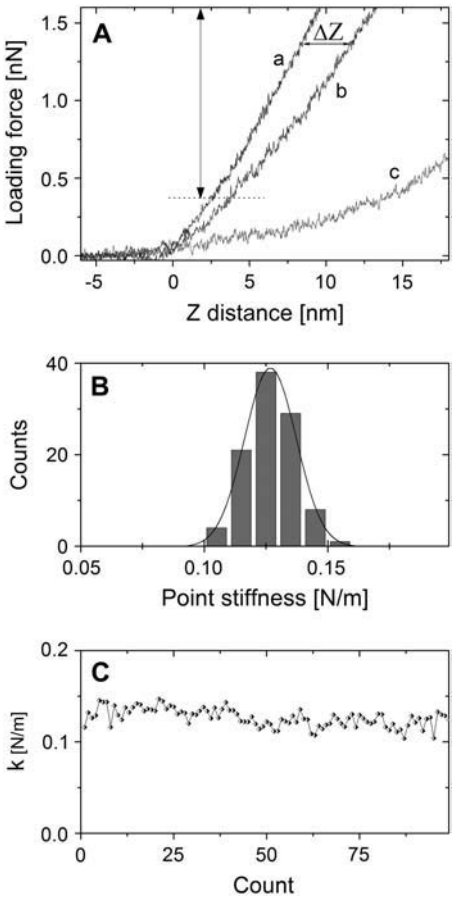

FIGURE 3 Measuring the point stiffness of the virus by indentation-type experiments. (*A*) Typical force-distance curves of cantilever deflection (curve *a*), natively proportioned/sized mature virus attached to HMDS-pretreated glass slide (curve *b*), and flattened mature virus attached to mica (curve *c*). All curves were shifted along the *z* axis to set the tip-sample contact point to a distance of zero. For each experiment, ~100 such curves were acquired. The virus indentation depth is defined as the difference between the *z* position of the virus and the deflection at a given loading force (labeled as ΔZ). For native-sized particles, there is a linear correlation between the loading force and the *z* distance (curve *b*). By contrast, a nonlinear force distance curve (*c*) is obtained from the indentation of flattened particles. The upper 75% segment of the curve that was used for the stiffness analysis is marked by a double-headed arrow. (*B*) Histogram and Gaussian-fitted curves of the individual measured point stiffness values derived from the consecutive force-distance curves of a single mature virus particle attached to a microscope's glass slide. (*C*) The individual measured point stiffness values obtained for the mature virus shown in panel *B*, during a single experiment against the experiment number (count). Such plots together with an analysis of the narrow distribution of the individual measured spring constants demonstrate that the virus did not undergo a significant irreversible deformation during the indentation measurements.

repeated application of force may irreversibly damage the sample. Therefore, for each measurement consisting of nearly 100 force-distance curves we verified that the virus did not undergo irreversible deformation. The measured point stiffness derived from these ~100 curves was plotted as a function of the measurement number, and as a histogram to which a Gaussian curve was fitted (Fig. 3, *B* and *C*). The distribution of the measured stiffness within a single experiment is shown for a mature virus particle in Fig. 3 *B*. Similar distribution is obtained for immature particles (data not shown). During each experiment, the measured stiffness values derived from the individual force-distance curves were found to distribute normally around a mean, which suggests that the virus did not undergo irreversible deformation during measurement.

The effect of maturation on virus mechanical properties

Although maturation has no effect on the appearance of the virus imaged by AFM, it results in significant internal morphological changes when visualized by EM (5–9). We find that virus maturation has a dramatic effect on its point stiffness. In fact, cantilevers used to indent mature virus particles (DNP) were too soft for use on immature particles, which could only be indented by significantly stiffer cantilevers (MLCT-AUHW). The effect of maturation on virus mechanical properties is presented in Fig. 4 where the averaged measured stiffness obtained from the complete dataset is shown. Our dataset includes virus particles with diameters ranging from 80 to 150 nm; however, their stiffness values do not correlate with their height, as indicated by Fig. 4 (*inset*). The scatter in the measured stiffness values is likely to reflect variations from one retrovirus particle to the next. The averaged measured stiffness of mature virus particles is 0.13 N/m ($SD = 0.05$, $n = 29$). Immature particles are almost three times stiffer than mature particles, with an averaged measured point stiffness of 0.33 N/m ($SD = 0.13$, $n = 24$). Student's *t*-test showed this difference in

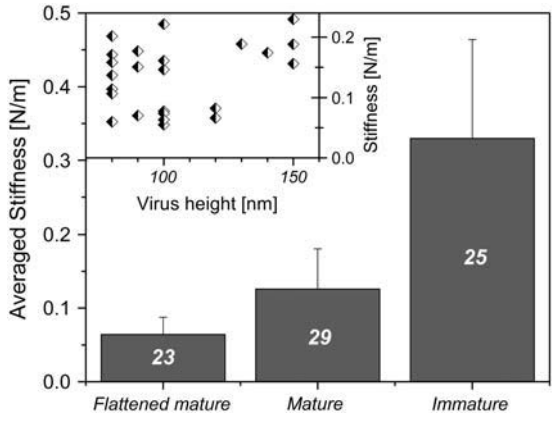

FIGURE 4 The averaged measured point stiffness of MLV virus. Each value was calculated as the average of ~100 force-distance curves obtained from individual virus particles. The average stiffness values derived from all of the measurements are 0.06 N/m ($SD = 0.02$, $n = 23$), 0.13 N/m ($SD = 0.05$, $n = 29$), and 0.33 N/m ($SD = 0.13$, $n = 25$), for flattened mature, mature, and immature virus particles, respectively. Number in columns indicates number of virus particles analyzed. The inset shows a scatter plot of the measured point stiffness values as a function of the mature virus particles' diameters. Similar plot is obtained for immature virus (not shown).

stiffness values to be significant ($P < 0.0001$ at 99.9% confidence level). Using the equation presented in Materials and Methods, we calculated that the average stiffness values of mature and immature virus particles are 0.31 N/m and 0.68 N/m, respectively.

To an outside observer the internal structure is hidden. Only average stiffness can be sensed. The material property that can be extracted from the experiment is the average Young's modulus. To estimate the average Young's moduli (E) of the virus particles from the measured virus stiffness, we assume that the mechanical behavior of the virus can be described as a homogeneous, linear elastic material and we ignore the different constituents of the shell. Within this framework we have modeled our indentation experiments by using a finite-element method. Mature and immature virus particles were modeled as hollow spheres with an outer radius of 50 nm and inner radius of 46 and 30 nm for the mature and immature states, respectively (the lipid bilayer is ignored since it is relatively soft). Virus dimensions were adopted from an MLV electron cryo-microscopy study (9). Fig. 5 shows the contours of the models of the mature and immature virus particles and the models' deformation under the indenter pressure. Fig. 6 shows their corresponding state of stress. A considerable difference in the mechanical response of the two models under indentation can be observed. In the immature state the deformation is absorbed in the vicinity of the indenter (Fig. 5 *A*). Compressive stresses are localized in the contact region (resembling Hertzian contact) (Fig. 6 *A*). On the other hand, in the mature virus model a large portion of the structure deflects under the indenter (Fig. 5 *B*). Nonvanishing stresses persist throughout the shell thickness, changing direction to tensile stress in the inner surface under the indenter and in the outer surface far from the indenter. This state of stress resembles the bending of a thin shell (Fig. 6 *B*). As a consequence the movement of the indenter comprises of the sum of a nonlocal deflection of the thin shell under an applied load and local indentation into the material. This means that the apparent stiffness of the shell is less than would be observed with a thick-walled sphere made of the same material. To obtain the experimentally observed mechanical stiffnesses of the two states of the virus requires that the Young's modulus of the mature state be 4.4-times larger than the modulus of the immature state, as listed in Table 1. Indeed, when the Young's modulus of the

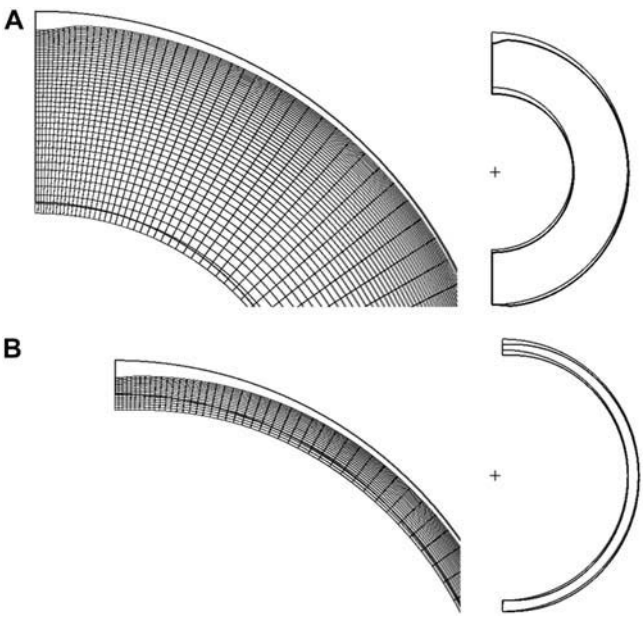

FIGURE 5 Finite element simulation for indentation of immature and mature virus particles. The simulation was done on a sector of the spherical particles of radii proportional to 50 nm. The shapes of an immature ($t =$ 20 nm) and a mature ($t = 4$) virus models (t is the shell's thickness) deformed under the pressure of the indenter are shown in *A* and *B*, respectively. The models are situated on a flat surface at the bottom and indented on the top side to a 2 nm displacement of the indenter, shown in detail in the left-side figures. The contours of the virus before the indentation are shown by solid lines.

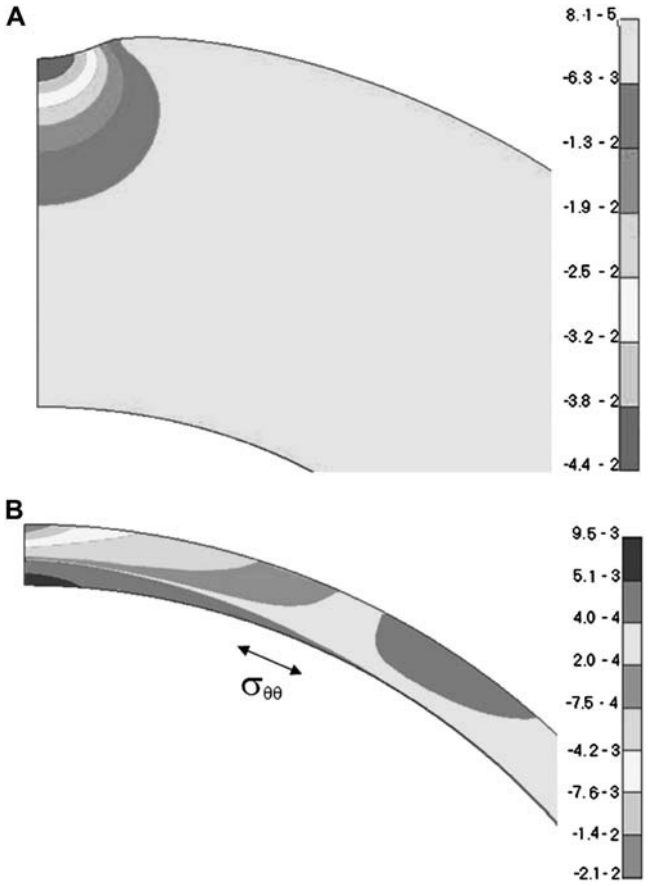

FIGURE 6 Maps of representative stress components in the immature and mature models. (*A*) The minimum principal stress (maximum compressive component oriented nearly parallel to the z axis) beneath the indenter in the immature virus model. Note the sharp decay of the stress with distance from the contact area. (*B*) The tangential stress $\sigma_{\theta\theta}$ in the mature virus model (stress in the direction indicated in the figure). A tensile stress persists far from the contact area corresponding to the bending of the shell. The scale bars represents the stress in MPa. Animated simulations are available online as Supplementary Material.

TABLE 1 The mechanical properties of immature and mature virus particles

State	R_{ext} [nm]	Wall thickness [nm]	K [N/m]	Estimated E [GPa]
Immature	50	20	0.68	0.233
Mature	50	4	0.31	1.027

mature state is taken to be equal to the modulus of the immature state, a stiffness of 0.07 N/m is calculated, instead of the measured 0.31 N/m. The simulation results were changed by only 16% when the indenter diameter was increased to 60 nm (the upper value indicated by the manufacturer). This control demonstrates that our model tolerates possible indenter variations, and thus supports the finite element simulation results. Fig. 7 shows that the simulated force-deformation curves agree with the experimental data. It is interesting to note that the simulated response of the thin shell is linear while the stiffness of the thick-walled sphere gradually increases, since the deformation spreads on the two poles of the sphere to an increasing volume of material. This causes an increase in the apparent stiffness from ~0.3 N/m at 0–0.25 nm deflection, to a nearly constant value of 0.9 N/m, along the second-half of the simulated indentation (Fig. 7). The difference in the shape of the curves is, however, in the limit of the resolution of our experiments, and therefore could not be verified experimentally.

In the mature form, the virus shell is composed of assembled MA proteins, while the shell of the immature form is composed of uncleaved Gag proteins. The mechanical properties of such a supramolecular shell are dictated by its thickness as well as the interactions between its building blocks, or in the case of virus shell, the strength of MA or

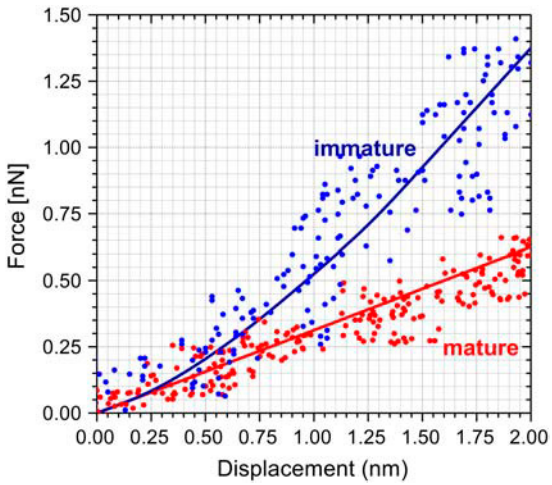

FIGURE 7 Simulated (*lines*) versus experimental (*dots*) force-deformation curves of the mature (*blue*) and immature (*red*) virus models for the best-fitted Young's moduli, listed in Table 1. The response of the thin shell in the mature state is linear whereas the stiffness of the thick wall of the immature state gradually increases since the deformation spreads on the two poles of the sphere to an increasing volume of material.

Gag protein-protein interactions. The simplest model of the structure of mature and immature particles would be one in which the MA and Gag proteins are plain rods, differing only in their length, with homogenous interactions throughout the length of the rods. In this model, the observed effect of maturation on virus point stiffness would only be due to the difference in thickness between the mature and immature shells. In contrast to point stiffness, the Young's modulus is an intrinsic material property, independent of geometry; thus it does not depend on the thickness of the virus shell. Therefore, in the above simplified model, if the two states of the virus were made of materials with the same properties, the Young's moduli would be equal. In contrast to this, the differences in the measured stiffness indicate different mechanical properties of the material in the two states of the virus. These results are quite compatible with the known complexity of retrovirus particle structure. For example, in the immature virus there is a poorly ordered layer, the pp12 domain, between the MA and CA domains (9). It is expected that such a poorly ordered layer's contribution to the overall stability of the shell will be small or nil. The CA domain in the immature shell has the largest contribution to the Gag protein-protein interactions (23,24), and therefore is expected to increase the stability of the shell. In contrast, assembly of the immature shell from full length Gag proteins is likely to include steric hindrance which, in turn, may reduce the overall stability of the shell. Moreover, once the individual domains are cleaved from Gag, they undergo structural changes which affect their binding to neighboring proteins. Indeed, we find a significant difference between the Young's modulus of the mature and immature virus, which represents changes in the shell's composition and strength. Interestingly, the modulus of the mature state is 4.4-fold higher than the immature one. This result suggests that the strength per length unit of MA protein-protein interactions is larger than that of Gag-Gag interactions. The increased modulus of the mature state may serve to maintain the virus stability despite the shell thickness reduction during maturation. Moreover, the finite-element simulation shows that in the immature virus, external forces are absorbed locally, while inducing large structural deformations in the mature virus (Fig. 6). Such a mechanical behavior for the immature virus increases its durability, and is likely to protect the nascent virus particle on its way to spread infection.

The finite-element simulation also allows us to compare the stiffness of MLV with other biological samples. Our calculation shows that MLV particles in the mature and immature forms are both stiffer than phospholipid vesicles (~2 MPa) (25) and nearly three orders-of-magnitude stiffer than mammalian cells (KPa range) (26–28). However, they are significantly softer than peptide nanotubes (~19 GPa) (17), but similar to bacteriophage capsids (~1.8 GPa) (16), and microtubules (~1 GPa) (15).

Future work will be focused on characterization of the mechanical properties of virus particles in which individual

Gag cleavage sites are genetically blocked. These studies are expected to provide insights on the contribution of each domain to the overall stability of the virus structure, and into Gag protein-protein interactions in the various maturation states.

The virus shell

Virus particles deposited on positively charged mica exhibit a lower height and different mechanical properties than native-shaped particles. These flattened virions are softer than native-sized mature particles (Fig. 4), with an averaged measured point stiffness value of 0.06 N/m ($SD = 0.02$, $n = 23$). Interestingly, the flattened mature virus is practically identical to the flattened immature form in height and in contrast to native-sized particles, in its mechanical properties (data not shown). The above results suggest that the deformation of the flattened virus induces structural alterations. Further insight into the virus structure can be obtained from the shape of the force-distance curves (Fig. 3 *A*). In the force-distance curves of native-sized particles (mature and immature), there is practically a linear correlation between the loading force and the *z* displacement. Thus, the point stiffness values derived from these force-distance curves are constant and independent of loading force. Such a correlation is typical for the indentation of shells (as long as the indentation depth is smaller than the shell thickness) (29). By contrast, a nonlinear force-distance curve is obtained from the indentation of flattened particles. This is due to the point stiffness increasing with loading force, and suggests a broken shell. A similar nonlinear correlation is obtained during indentation of structures, such as lipid vesicles (25,30), that lack a rigid shell structure. We therefore conclude that an excessive binding force between the virus and a rigid substrate (mica) deforms the virus. This excessive force is presumably larger than the mechanical differences between the mature virus and the stiffer immature virus particles, and is sufficient to collapse their structure to such a degree that they become indistinguishable.

We next measured the effect of directly applying an excessive force with the AFM on an individual virus particle attached to a glass slide. In these experiments, after acquisition of a few tens of force-distance curves, the loading force was gradually increased to its maximal level. The force was then reduced back to its initial value, and more force-distance curves were acquired. As seen in Fig. 8 *A*, at the beginning of the experiment the force-distance curve's shape was typical of a mature particle. However, after application of excessive force, the mechanical properties of the virus changed (Fig. 8 *A*) while the height of the virus remained unaffected. These changes were manifested not only in a reduced point stiffness value, but also in a loss of the linear nature of the force-distance curve. In several experiments, the point stiffness of the particle abruptly dropped (*arrow* in Fig. 8 *B*), probably due to structural fatigue induced by the repetitive stress. All of the above results strongly support the hypothesis that the mature virus in its native form has an intact rigid shell structure underneath its membrane.

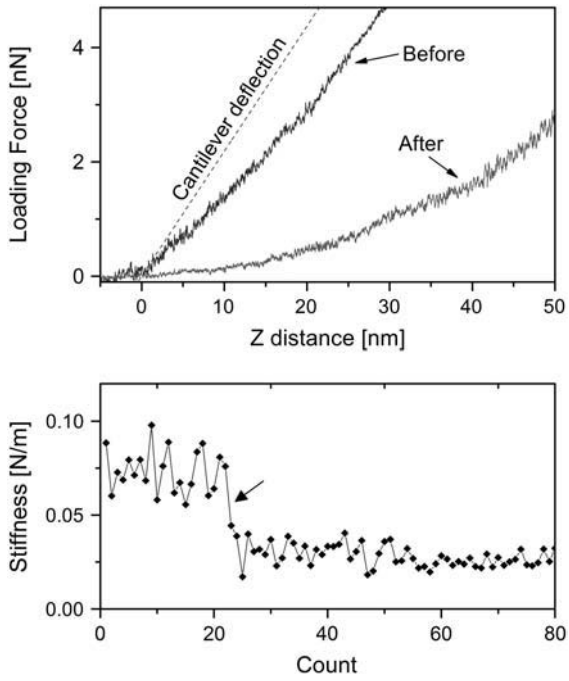

FIGURE 8 Breakage of the virus shell by force application. (*A*) Force-distance curve of an intact mature virus (*Before*), and the curve of the same virus after application of intense force (*After*). For reference, the cantilever deflection is plotted (*dashed black line*). (*B*) Eighty individual measured point stiffness values obtained for a mature virus during a single experiment against the experimental number (*count*). The maximal loading force was kept constant during the entire length of the experiment. After 20 repetitive curves, there was an abrupt drop (marked with an *arrow*) in the stiffness of the virus particle.

CONCLUSIONS AND IMPLICATIONS

Previous EM studies provided important data on the morphological changes that occur during maturation. Our data demonstrate, for the first time, a clear difference in the mechanical properties of mature compared to immature virus particles. Based on our findings, we speculate that virus particles' adoption of different sets of mechanical properties at different stages in their maturation process is of importance to their replication. For example, it is possible that during budding, assembly of the Gag rigid shell below the cell membrane stabilizes the highly curved nascent virus. In contrast, such a rigid shell might inhibit subsequent entry into or dissociation within a target cell. Thus, the overall weakening of the viral structure that we have detected here may play an essential role in the infectious process.

At present, it is not clear from the literature whether MA proteins form a lattice under the membrane of a mature retrovirus particle. Our results provide strong supporting

evidence for the existence of a rigid shell below the membrane of the intact mature virus, which is presumably composed of MA molecules. We show that the shell is brittle and can be broken under excessive loading forces. The existence of such a shell poses a challenge for our current understanding of the fundamental mechanism for viral entry. Undoubtedly, for infectivity, this MA shell must break to enable content mixing between the virus and the cell after membrane fusion. Presently, it is not known whether the virus shell collapses upon binding to the cell membrane, as it does when the virus is deposited on mica by electrostatic interactions, or whether it enters the cell as an intact shell that slowly disassembles at a later stage. Our current efforts are focused on addressing such questions.

SUPPLEMENTARY MATERIAL

An online supplement to this article can be found by visiting BJ Online at http://www.biophysj.org.

We thank Michael S. Kay for helpful discussions and a critical review of the manuscript, Dr. Etai Shipgel, Nelia Shechter from Alomone Labs Ltd., and Jane Mirro for technical assistance.

This work was supported by a grant from the Eisenberg-Keefer Fund for New Scientists, the Kimmelman Center for Macromolecular Assemblies, and in part by the Intramural Research Program of the National Institutes of Health, National Cancer Institute, Center for Cancer Research. I.R. is the incumbent of the Robert Edward and Roselyn Rich Manson Career Development Chair.

REFERENCES

1. Shields, A., W. N. Witte, E. Rothenberg, and D. Baltimore. 1978. High frequency of aberrant expression of Moloney Murine Leukemia Virus in clonal infections. *Cell.* 14:601–609.
2. Wills, J. W., and R. C. Craven. 1991. Form, function, and use of retroviral Gag proteins. *AIDS.* 5:639–654.
3. Swanstrom, R., and J. W. Wills. 1997. Synthesis, assembly, and processing of viral proteins. *In* Retroviruses. J. M. Coffin, S. H. Hughes, and H. E. Varmus, editors. Cold Spring Harbor Laboratory, Plainview, NY. 263–334.
4. Coffin, J. M., S. H. Hughes, and H. E. Varmus. 1997. Retroviruses. Cold Spring Harbor Laboratory, Plainview, NY.
5. Katoh, I., Y. Yoshinaka, A. Rein, M. Shibuya, T. Odaka, and S. Oroszlan. 1985. Murine Leukemia Virus maturation: protease region required for conversion from ''immature'' to ''mature'' core form and for virus infectivity. *Virology.* 145:280–292.
6. Peng, C., B. K. Ho, T. W. Chang, and N. T. Chang. 1989. Role of Human Immunodeficiency Virus Type 1-specific protease in core protein maturation and viral infectivity. *J. Virol.* 63:2550–2556.
7. Stewart, L., G. Schatz, and V. M. Vogt. 1990. Properties of avian retrovirus particles defective in viral protease. *J. Virol.* 64:5076–5092.
8. Voynow, S. L., and J. M. Coffin. 1985. Truncated Gag-related proteins are produced by large deletion mutants of Rous Sarcoma Virus and form virus particles. *J. Virol.* 55:79–85.
9. Yeager, M., E. M. Wilson-Kubalek, S. G. Weiner, P. O. Brown, and A. Rein. 1998. Supramolecular organization of immature and mature Murine Leukemia Virus revealed by electron cryo-microscopy: implications for retroviral assembly mechanisms. *Proc. Natl. Acad. Sci. USA.* 95:7299–7304.
10. Hansen, M., L. Jelinek, R. S. Jones, J. Stegeman-Olsen, and E. Barklis. 1993. Assembly and composition of intracellular particles formed by Moloney Murine Leukemia virus. *J. Virol.* 67:5163–5174.
11. Yoshinaka, Y., and R. B. Luftig. 1977. Properties of a P70 proteolytic factor of murine leukemia viruses. *Cell.* 12:709–719.
12. Bozec, L., and M. Horton. 2005. Topography and mechanical properties of single molecules of type I collagen using atomic force microscopy. *Biophys. J.* 88:4223–4231.
13. Radmacher, M. 1997. Measuring the elastic properties of biological samples with the AFM. *IEEE Eng. Med. Biol. Mag.* 16:47–57.
14. Stolz, M., R. Raiteri, A. U. Daniels, M. R. VanLandingham, W. Baschong, and U. Aebi. 2004. Dynamic elastic modulus of porcine articular cartilage determined at two different levels of tissue organization by indentation-type atomic force microscopy. *Biophys. J.* 86: 3269–3283.
15. Ivanovska, I. L., P. J. de Pablo, B. Ibarra, G. Sgalari, F. C. MacKintosh, J. L. Carrascosa, C. F. Schmidt, and G. J. Wuite. 2004. Bacteriophage capsids: tough nanoshells with complex elastic properties. *Proc. Natl. Acad. Sci. USA.* 101:7600–7605.
16. de Pablo, P. J., I. A. T. Schaap, F. C. MacKintosh, and C. F. Schmidt. 2003. Deformation and collapse of microtubules on the nanometer scale. *Phys. Rev. Lett.* 91:0981011–0981014.
17. Kol, N., L. Adler-Abramovich, D. Barlam, R. Z. Shneck, U. Gazit, and I. Rousso. 2005. Self-assembled peptide nanotubes are uniquely rigid bio-inspired supramolecular structures. *Nano Lett.* 5:1343–1346.
18. Fu, W., and A. Rein. 1993. Maturation of dimeric viral-RNA of Moloney Murine Leukemia-virus. *J. Virol.* 67:5443–5449.
19. Graham, F. L., and A. J. van der Eb. 1973. A new technique for the assay of infectivity of human adenovirus 5 DNA. *Virology.* 52: 456–467.
20. Hutter, J. L., and J. Bechhoefer. 1993. Calibration of atomic-force microscope tips. *Rev. Sci. Instrum.* 64:1868–1873.
21. Bueckle, H. 1973. The Science of Hardness Testing and its Research Applications. J. W. Westbrook and H. Conrad, editors. American Society for Metals, Materials Park, Ohio.
22. Persch, G., C. Born, and B. Utesch. 1994. Nano-hardness investigations of thin-films by an atomic-force microscope. *Microelectr. Eng.* 24:113–121.
23. Ako-Adjei, D., M. C. Johnson, and V. M. Vogt. 2005. The retroviral capsid domain dictates virion size, morphology, and coassembly of Gag into virus-like particles. *J. Virol.* 79:13463–13472.
24. Wang, M. Q., and S. P. Goff. 2003. Defects in virion production caused by mutations affecting the C-terminal portion of the Moloney Murine Leukemia Virus capsid protein. *J. Virol.* 77:3339–3344.
25. Liang, X. M., G. Z. Mao, and K. Y. S. Ng. 2004. Probing small unilamellar Egg-PC vesicles on mica surface by atomic force microscopy. *Colloids Surf. B Biointerfaces.* 34:41–51.
26. Byfield, F. J., H. Aranda-Espinoza, V. G. Romanenko, G. H. Rothblat, and I. Levitan. 2004. Cholesterol depletion increases membrane stiffness of aortic endothelial cells. *Biophys. J.* 87:3336–3343.
27. Lieber, S. C., N. Aubry, J. Pain, G. Diaz, S. J. Kim, and S. F. Vatner. 2004. Aging increases stiffness of cardiac myocytes measured by atomic force microscopy nanoindentation. *Am. J. Physiol. Heart Circ. Physiol.* 287:H645–H651.
28. Zelenskaya, A., J. B. de Monvel, D. Pesen, M. Radmacher, J. H. Hoh, and M. Ulfendahl. 2005. Evidence for a highly elastic shell-core organization of cochlear outer hair cells by local membrane indentation. *Biophys. J.* 88:2982–2993.
29. Landau, L. D., and E. M. Lifshitz. 1986. Theory of Elasticity. Pergamon Press, New York.
30. Liang, X. M., G. Z. Mao, and K. Y. S. Ng. 2004. Mechanical properties and stability measurement of cholesterol-containing liposome on mica by atomic force microscopy. *J. Colloid Interface Sci.* 278:53–62.